Contrib Mineral Petrol (2007) 154:409–427
DOI 10.1007/s00410-007-0200-1

ORIGINAL PAPER

Lithosphere formation in the central Slave Craton (Canada): plume subcretion or lithosphere accretion?

Sonja Aulbach · William L. Griffin · Norman J. Pearson · Suzanne Y. O'Reilly · Buddy J. Doyle

Received: 27 September 2006 / Accepted: 2 April 2007 / Published online: 8 May 2007

Abstract Major-element compositions of minerals in peridotite xenoliths from the Lac de Gras kimberlites provide constraints on the mode of lithosphere formation beneath the central Slave Craton, Canada. Magnesia contents of reconstructed whole rocks correlate positively with NiO and negatively with CaO contents, consistent with variable partial melt extraction. Alumina and Cr_2O_3 contents are broadly positively correlated, suggestive of melt depletion in the absence of a Cr–Al phase. Garnet modes are high at a given Al_2O_3 content (a proxy for melt depletion), falling about a 7 GPa melt depletion model. These observations, combined with high olivine Mg# and major-element relationships of FeO-poor peridotites (<7.5 wt%) indicative of melt loss at pressures >3 GPa (residual FeO content being a sensitive indicator of melt extraction pressure), and similar high pressures of last equilibration (~4.2 to 5.8 GPa), provide multiple lines of evidence that the mantle beneath the central Slave Craton has originated as a residue from high-pressure melting, possibly during plume subcretion. Apparent low melt depletion pressures for high-FeO peridotites (>7.5 wt%) could suggest formation in an oceanic setting, followed by subduction to their depth of entrainment. However, these rocks, which are characterised by low SiO_2 contents (<43 wt%), are more likely to be the result of post-melting FeO-addition, leading to spuriously low estimates of melt extraction pressures. They may have reacted with a silica-undersaturated melt that dissolved orthopyroxene, or experienced olivine injection by crystallising melts. A secular FeO-enrichment of parts of the deep mantle lithosphere is supported by lower average Mg# in xenolithic olivine (91.7) compared to olivine inclusions in diamond (92.6).

Keywords Mantle peridotite origins · Mantle melting · Plume mantle · Subcontinental lithosphere formation · Lac de Gras lithospheric mantle

Communicated by T.L. Grove.

S. Aulbach · W. L. Griffin · N. J. Pearson · S. Y. O'Reilly
GEMOC ARC National Key Centre,
Department of Earth and Planetary Sciences,
Macquarie University,
NSW 2109 North Ryde, Australia

Present Address:
S. Aulbach (✉)
Earth and Atmospheric Sciences, University of Alberta,
Edmonton, AB, Canada T6G 2E3
e-mail: saulbach@els.mq.edu.au

W. L. Griffin
CSIRO Exploration and Mining,
N. Ryde, NSW 2113, Australia

B. J. Doyle
Lithosphere Services, 4009 Edinburgh Street,
Burnaby, BC, Canada V5C 1R4

Introduction

Peridotites from the subcontinental lithospheric mantle (SCLM) are typically depleted in magmaphile elements relative to fertile mantle. This depletion is related to partial melting events that led to the formation and stabilisation of the lithosphere (e.g. Boyd and McCallister 1976; Jordan 1988; Walter 1998). While there is general agreement that partial melting leads to residues with decreased density and hence to lithosphere stabilization, there are two main competing hypotheses regarding the formation of ancient

depleted SCLM: (1) by successive stacking of oceanic lithosphere, through underthrusting or subduction at convergent margins, or (2) by plume subcretion. Both modes of cratonic lithosphere formation may have operated in the Archaean (Herzberg 1999; Griffin et al. 2004).

Arguments in favour of the stacking hypothesis include (1) minor- and major-element contents and relationships in peridotites that seem to require shallow melting (in the spinel stability field) (Stachel et al. 1998; Canil 2004) and (2) apparent low pressures of melt extraction that contrast with higher pressures of last equilibration for many mantle samples (Herzberg 1999).

By contrast, the plume model is successful in explaining (1) the occurrence of high-pressure large-volume melts (komatiites) and a complementary depletion in cratonic peridotites (e.g. Herzberg 1995, 1999; Walter 1998) and (2) the formation of low-FeO residual Archaean SCLM that is buoyant enough to remain isolated from the convecting mantle over billions of years (Herzberg 1995; Abbott et al. 1997; Griffin et al. 1999a).

It has previously been suggested that at least the deeper parts of the lithospheric mantle beneath the central Slave Craton formed by plume subcretion beneath a pre-existing, shallow ultra-depleted lithosphere (Griffin et al. 1999b, 2004). This would explain the the marked stratification of the mantle lithosphere beneath parts of the Slave Craton, with predominantly lherzolitic material at depths >140 km, the occurrence of abundant diamonds containing typical lower-mantle assemblages (Griffin et al. 1999b; Davies et al. 1999), the strong heterogeneity in the distribution of rock types beneath the different mantle sections in the shallow layer, contrasting with a remarkable uniformity in the deeper layer (Griffin et al. 2004; Poudjom Djomani et al. 2005) and the supra-chondritic initial $^{187}Os/^{188}Os$ of isochronous sulfide inclusions in xenocrystic olivine from the central Slave Craton, which may be the signature of a high-Re/Os source, such as the lower mantle or outer core (Aulbach et al. 2004).

Others have challenged this interpretation, citing high Cr/Al ratios in garnet inclusions in diamond from the central Slave Craton; these ratios appear to require previous depletion within the spinel stability field, followed by subduction to greater depth, as spinel is the only mantle phase imparting a large bulk $D_{Cr/Al}$ (Stachel et al. 2003; Canil 2004; Tappert et al. 2005). These authors advocate a ''mantle stacking'' model to account for the strong layering of the mantle beneath the central Slave Craton, in accord with seismic reflection profiles of the western part of the craton that were interpreted as the result of several shallow subduction events (Bostock 1998; Cook et al. 1999). It is suggested that during these events, 70 km-thick Slave Craton Archaean lithosphere was successively underplated by the younger, Proterozoic lithosphere of terranes accreted to the western margin of the Slave Craton. A tenuous correlation between between a major change in the chemical composition of garnets from the southwestern margin of the craton with one of the discontinuities reported by Bostock (1998) was interpreted in terms of this stacking model (Carbno and Canil 2002).

We have carried out an in-depth investigation of variably depleted peridotite xenoliths from the Lac de Gras kimberlites in order to place further constraints on the origin of the deep mantle layer, using detailed modal, major-element and depth relationships. The present study focuses on a larger suite of bigger xenolith samples, including pipes not previously sampled (A418, A841), that has become available in drill core since the first studies of Griffin et al. (1999b) and Pearson et al. (1999).

Geological setting

The Slave Craton consists of two major basement units (1) the 4.0–2.9 Ga Central Slave Basement Complex (CSBC; Bleeker et al. 1999) in the west and (2) a Neoarchaean (<2.8 Ga), isotopically juvenile domain in the east (Fig. 1). The origin of these domains is not well constrained and interpretations range from arc-continent collision (Kusky 1989; Davis and Hegner 1992) to formation of the eastern domain by attenuation and modification of the Mesoarchaean lithosphere (Bleeker 2003). The reader is referred to Davis et al. (2003) for a recent detailed overview of the crustal evolution in the region.

Researchers working on mantle samples from different parts of the craton have found distinct mantle suites and spatial distributions of mantle rock types in the lithosphere column that point to different origins and metasomatic histories (Griffin et al. 1999b, 2004; Grütter et al. 1999; Kopylova et al. 1999; MacKenzie and Canil 1999; Pearson et al. 1999; Carbno and Canil 2002; Kopylova and Caro 2004; Menzies et al. 2004). The basic structure recognised for the Slave Craton is one of a strongly stratified mantle in the craton centre, where an ultra-depleted shallow layer is underlain by a more fertile but still generally depleted deep layer (Fig. 1 inset).

With the exception of Drybones Bay near the southwestern part of the craton edge where the sharp layering is still evident (Carbno and Canil 2002), the transition between the layers is smeared out or layering is absent towards the craton margin (Griffin et al. 1999b, 2004; Poudjom Djomani et al. 2005). The mantle beneath the Jericho kimberlite, in the north central part of the craton, is unique in that it contains a distinct boundary at 160–190 km depths, where a sizable proportion of high-temperature magmatic pyroxenites and porphyroclastic

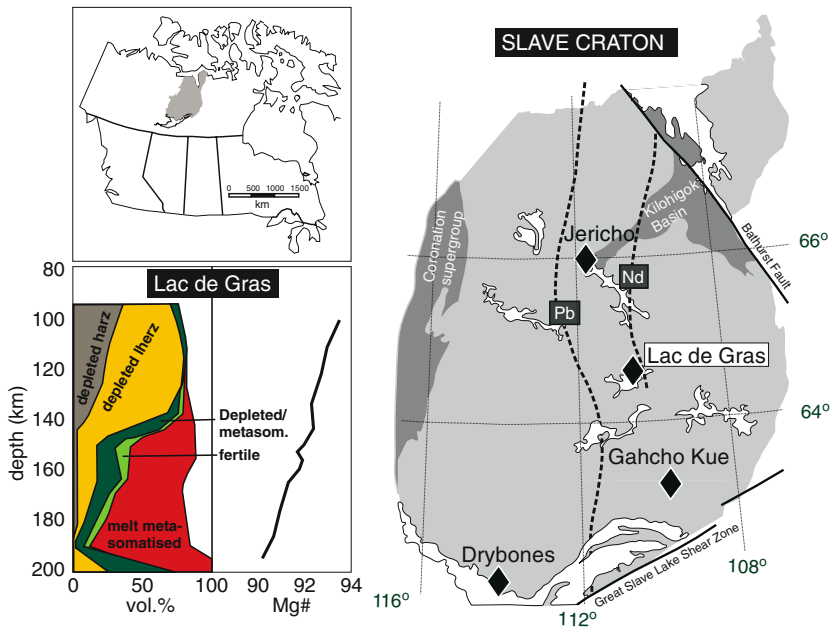

Fig. 1 Map of the Slave Craton showing Pb and Nd isotope lines separating Hadean to Meso-Archaean basement in the west from <2.8 Ga rocks in the east (after Davis et al. 2003; see text for details). *Top left* shows location of Slave Craton in northwestern Canada, *bottom left* shows distribution of rock types and forsterite content in olivine against depth in the Lac de Gras area (after Fig. 6 in Griffin et al. 2004)

peridotites occur (Kopylova et al. 1999). This mantle section also appears to more be strongly modified by metasomatism than others in the Slave province; this may reflect its position near a major translithospheric fault marked by the Kilohigok Basin (Poudjom Djomani et al. 2005). In contrast, the southeastern Slave Craton stands out in terms of its thicker and cooler mantle lithosphere compared to other Slave mantle terranes (Kopylova and Caro 2004).

A significant north-south trending dichotomy in the Slave Craton is recognised from basement isotope data (Davis and Hegner 1992). Many kimberlites lie in the younger, eastern domain, but appear to have sampled older lower crust and mantle, consistent with an east-dipping trans-lithospheric boundary dating back to 2.7 Ga craton amalgamation (Grütter et al. 1999; Irvine et al. 2003; Aulbach et al. 2004). Strong gradients in the gravity signature and mechanical strength of the lithosphere follow the Nd isotope boundary (Poudjom-Djomani et al. 2005).

The Lac de Gras kimberlites that entrained the samples studied here have sampled the strongly layered lithosphere beneath the central part of the craton. Re–Os data for some sulfides from the deep layer lie on a 3.27 ± 0.34 Ga isochron, which is interpreted as the formation age of this layer (Aulbach et al. 2004). A similar age (3.52 ± 0.17 Ga) was obtained for sulfide inclusions in diamonds from the shallow mantle layer in the same area (Westerlund et al. 2006).

Sample preparation and analytical techniques

All analytical work was carried out in the GEMOC National Key Centre at Macquarie University (http://www.es.mq.edu.au/GEMOC/). Mineral modes in the present study were obtained by point-counting on standard sections using an optical microscope. The upper limit for the associated errors was assessed following Solomon (1963), using average grain sizes where reasonable. For porphyroclastic varieties, the size of the porphyroclasts was used; if a continuum of grain sizes was observed, the largest grain size was used. Therefore, the resulting uncertainties are maximal and may in most cases be smaller. For the older unpublished studies, exact numbers of points counted are not available; the policy was to count 500 points and this number was used in the uncertainty calculation.

In situ major-element analyses were performed using a CAMECA Camebax SX50 electron microprobe with 15 kV acceleration voltage and counting times of 10 s on the peak, 5 s on each side of the background. Kimberlite-borne xenoliths are often infiltrated by the host melt, which corrupts in particular the incompatible major- and trace-element budget (e.g. Boyd et al. 1997). This can make point-counted modes more reliable than those computed from bulk analyses (Kopylova and Caro 2004). Whole-rock compositions were reconstructed using mineral compositions weighted by modal abundance. The uncertainty in mineral modes, due to the sometimes coarse grain size relative to the sample size and the non-uniform distribution of the principal minerals on thin section scale (e.g. Cox et al. 1987), has been used to calculate uncertainties in the composition of the reconstructed whole rock and was taken to be the square root of the sum of squared standard deviations of the modes (this is an upper limit as mineral modes are not independent variables).

Typically, three to five grains of each mineral were analysed in a traverse of six spots that included both cores and rims, and porphyroclasts and neoblasts where applicable, to monitor intra- and inter-grain variations. With the exception of geothermobarometric calculations, where rim compositions are used, only core compositions are described, used in whole rock reconstructions and discussed, to exclude compositions possibly affected by late diffusion, for example due to kimberlite infiltration.

Samples and classification

The samples are derived from pipes A154N, A154S, A418 and A841 of the Lac de Gras kimberlite cluster and are extremely fresh xenoliths extracted from drill core, mostly from depths of 150 to 470 m. The peridotites observed in drill core are overwhelmingly garnet lherzolites and harzburgites, with minor spinel peridotite, wehrlite and dunite present (Pearson et al. 1999); the latter two rock types are not included in this study. Petrographic details are given in Table 1. Most peridotites have medium- to coarse-grained equant to tabular, mostly foliated microstructure, with foliation defined by tabular olivine (nomenclature of Harte 1977). A second major microstructural group has non-fluidal, non-disrupted porphyroclastic microstructure. One sample (VR43461) consists entirely of garnet with interstitial or enclosed amoeboid spinel and another sample (YK3531) of garnet with interstitial, now altered, pyroxene. The garnet-spinel lherzolite consists almost entirely of cpx and garnet, which is probably due to non-representative sampling in this small xenolith (1 cm).

Olivine is present as large grains with curvilinear grain boundaries and undulose to lamellar extinction, with some formation of subgrain boundaries. Grain sizes are up to 10 mm, though mostly around 5 mm. In porphyroclastic varieties, the small grain sizes are represented by polygonal neoblasts. Like olivine, orthopyroxene is mostly anhedral with undulose extinction. Grain sizes are on the order of 1–4 mm, though grains up to 7 mm across have been observed. Clinopyroxene (cpx) forms discrete grains with curvilinear grain boundaries and sizes mostly around 1 mm, while garnet forms mostly polygonal to rounded grains with variable degrees of kelyphitisation and sizes between 1 and 5 mm. Spinel and sulfides are common accessory minerals ($\leq$ 1 vol.%). Ilmenite occurs in a Ca-saturated garnet harzburgite (YK1938). Representative examples of most rock types are illustrated in Pearson et al. (1999).

Modal abundances of cpx in 12 samples reveal that all are depleted lherzolites (<4 vol.%), i.e. harzburgites according to the classification of Streckeisen (1976). Because cpx may not be exposed in smaller samples due to sectioning effects, we use Ca–Cr relationships in garnet (see following section) to distinguish the following lithoypes: (1) Ca-undersaturated garnet harzburgites (cpx-free), (2) garnet lherzolites, where Ca-saturation of the garnet indicates equilibration with cpx regardless of whether or not cpx is exposed in thin section, (3) a garnet-spinel lherzolite and (4) a spinel lherzolite.

Mineral compositions

Garnet

The Cr–Ca relationships of cores are used to distinguish garnets that have equilibrated with both opx and cpx (Ca-saturated garnets) from those that have equilibrated with opx only (Ca-undersaturated garnets) (Fig. 2a). Several samples that fall on the lherzolite trend and have Cr_2O_3 contents >7 wt% plot at the low-Ca end at a given Cr content. Only three of the garnet peridotites contain Ca-undersaturated garnet. One of the Ca-undersaturated garnets (VR43461) has low contents of both CaO and Cr_2O_3 (0.99 and 2.34 wt%, respectively; Table 2). Garnet in garnet-spinel lherzolite (YK1923) is Cr-poor relative to its Ca-content compared to garnet in garnet lherzolites. Some peridotitic garnets have low CaO and Cr_2O_3 contents that overlap with the compositions of garnets in olivine-free pyroxenites (Pearson et al. 1999).

Garnets fall into two distinct groups with regard to TiO_2 contents: one group contains less than 0.46 wt% TiO_2 and a second group contains more than 0.66 wt% (Fig. 2b). The higher- TiO_2 group has on average lower MgO contents than the low-TiO_2 group, but FeO and other major element contents are virtually indistinguishable for the two. Ca-undersaturated garnets have the highest pyrope contents (100Mg/(Mg + Ca + Fe + Mn)) and some of the lowest TiO_2 contents of all garnets (i.e. mostly below the detection limit, 0.06 wt%).

Garnets in several samples have rim compositions with slightly lower Cr# (100Cr/(Cr + Al)) and similar or slightly higher Mg# (100Mg/(Mg + Fe)) than core compositions (Table 2).

Clinoyroxene (Cpx)

Like the garnets, cpx in garnet peridotites falls into two groups with regard to TiO_2 and Na_2O contents (Table 3), of which one group has $TiO_2 \geq 0.25$ and/or Na_2O contents $\geq$ 2.2 wt% (Table 3). Clinopyroxene in the garnet-spinel lherzolite (YK1923) has high Mg# (95.2) and low TiO_2 (<0.06 wt%) and Na_2O contents (0.7 wt%), whereas that in a spinel lherzolite (VR51067) has similarly high Mg# (95.5), but also the highest TiO_2 content measured

Table 1 Petrographic data, data sources and rock type classification for peridotites from the Lac de Gras kimberlites

Sample	Ref[a]	Rock type[b]	Microstructure[c]	Size (cm)	# Pts[d]	modal abundances (%)[e]								Trace phases[f]
						ol	2σ	opx	2σ	cpx	2σ	gt	2σ	
vr09356	3	gt lherz	NA	<1										
vr09358	3	gt lherz	NA	<1										
vr09359	3	gt lherz	NA	<1										
vr09361	3	gt lherz	Medium-tabular	1	500	52	(6)	37	(5)	4	(0.6)	7	(0.8)	
vr09364	3	gt lherz	NA	<1										
vr09366	3	gt lherz	NA	1										
vr09370	1	gt lherz	NA	<1										
vr09371	3	gt lherz	Coarse-equant	1.5	500	85	(8)	11	(0.5)			4	(0.3)	
vr09372	3	gt lherz	Coarse-equant	1.5										sp
vr19674 pg2	2	gt lherz	NA	<1										
vr19674 pg3	3	gt lherz	NA	<1										sp
vr40304	2	gt lherz	NA	<1										
vr40332	3	gt lherz	NA	<1										
vr40335	2	gt lherz	NA	<1										
vr40358	3	gt lherz	NA	<1										
vr40391	3	gt lherz	NA	<1										
vr43461	4	gt harz	Medium-granobl.	2										sp
vr43466	4	gt lherz	Coarse-tabular	5	1,027	81	(1)	15	(0.3)			4	(0.2)	sp
vr43467	4	gt lherz	Coarse-tabular	5	1,005	93	(3)	5	(0.6)	<1		2	(0.1)	sf
vr43499	4	gt lherz	Coarse-equant	1.5										
vr50851	3	gt lherz	Medium-tabular	2	500	76	(1)	18	(2)			6	(5)	sp
vr50855	3	gt lherz	NA	2.5										sp
vr50861	3	gt lherz	Medium-tabular	2	500	83	(1)	10	(2)	1	(8)	6	(2)	sp
vr50867	2	gt harz	NA	<1										
vr50875	3	gt lherz	Coarse-equant	2										sp
vr50879	1	gt lherz	NA	<1										
vr50882	1	gt lherz	NA	<1										
vr50885	1	gt lherz	NA	<1										
vr50886	3	gt lherz	NA	<1										
vr50904	1	gt harz	NA	<1										
vr50914	3	gt lherz	Porphyroclastic	1.5	500	71	(4)	22	(1)	1	(0.1)	6	(0.5)	sp
vr50933	1	gt lherz	NA	<1										
vr51067	4	sp lherz	Medium-tabular	2.5	1,012	83	(2)	16	(1)	<1				sp
vr51902	4	gt lherz	Coarse-equant	2										
vr67106	4	gt lherz	Medium-tabular	3	1,010	88	(1)	10	(0.5)			2	(0.2)	sp
vr67112	4	gt lherz	Coarse-tabular	4	1,031	75	(4)	25	(0.7)	1	(0.1)	<1		sp
vr67112b2	4	gt lherz	NA	1.5										
vr67125	4	gt lherz	Coarse-tabular	4	800	68	(3)	26	(1)	3	(0.2)	3	(0.2)	
yk1912	4	gt lherz	Porphyroclastic	2	378	69	(6)	16	(0.5)			15	(3)	
yk1917	4	gt lherz	Porphyroclastic	3	1,107	73	(8)	22	(0.3)	1	(0.2)	4	(0.6)	sf
yk1919	4	gt lherz	Porphyroclastic	1										
yk1920	4	gt lherz	Porphyroclastic	2.5	757	76	(7)	13	(1)	3	(0.2)	8	(1)	sp
yk1923	4	gt sp lherz	Medium-equant	1										
yk1938	4	gt lherz	Medium-equant	3	713	55	(2)	31	(1)			14	(0.6)	sf, ilm

Table 1 continued

Sample	Ref[a]	Rock type[b]	Microstructure[c]	Size (cm)	# Pts[d]	modal abundances (%)[e]								Trace phases[f]
						ol	2σ	opx	2σ	cpx	2σ	gt	2σ	
yk2471	4	gt lherz	Porphyroclastic	5	345	74	(5)	16	(0.6)	1	(0.1)	9	(0.7)	sf
yk2472	4	gt lherz	Porphyroclastic	5	1,063	79	(5)	18	(0.9)	<1		3	(0.2)	sp
yk2474	4	gt lherz	Coarse-tabular	5	1,504	75	(5)	17	(1.5)	1	(0.1)	7	(0.9)	sf

[a] *1* van Achterbergh et al. unpubl. data, *2* Pearson et al. unpubl. data, *3* Pearson et al. (1999), *4* this study

[b] Based on presence or absence of garnet and aluminous spinel, and Ca-saturation of garnet (see text for details); *gt* garnet, *sp* spinel, *lherz* lherzolite, *harz* harzburgite

[c] *Coarse* coarse-grained, *medium* medium-grained, *granobl.* granoblastic (classification of Harte 1977)

[d] Number of points counted for determination of modes

[e] 2σ are absolute values, calculated after Solomon (1963)

[f] *sp* Spinel, *sf* sulfide, *ilm* ilmenite

(0.5 wt%). Three peridotites have cpx with rim compositions that differ from cores, with rims having higher CaO contents. Sample VR43499 shows variability that is not resolvable in terms of core versus rim, with CaO contents ranging from 18.8 to 20.7 wt%, while garnet spinel lherzolite YK1923 has cpx with variable Al_2O_3 content (1.3–2.3 wt%).

Orthopyroxene (Opx)

Orthopyroxenes are homogeneous on grain and sample scales and generally have Mg# >92 (Table 4). Orthopyroxene in Ca-undersaturated harzburgite (VR50904) has higher Mg# (93.6) than opx in garnet lherzolites (mean 92.9). Orthopyroxenes in the garnet-spinel lherzolite (YK1923) and in the spinel lherzolite (VR51067) have Mg# at the high end of all opx analysed (93.0 and 93.4, respectively), but also have high Al_2O_3 contents. These samples have CaO contents at the low end of the range observed in all peridotites (0.29 and 0.36 wt%, respectively).

Olivine

Olivines in two samples show variability in terms of core versus rim compositions, with one having signifantly lower Mg# in the rim than in the core (YK1938). The Mg# of olivine in the Ca-undersaturated harzburgite is 92.5. Olivines coexisting with garnet that plots on the lherzolite trend, but at the CaO-poor end at a given Cr_2O_3 content, have higher Mg# (mean 92.5) than those coexisting with garnet having higher CaO content (mean 91.6). Olivine in garnet-spinel lherzolite has very high Mg# (92.9), and that in spinel lherzolite has the highest Mg# (93.4) (Table 5). Olivine in the garnet-spinel lherzolite records the highest NiO content by far (0.53 wt%).

Spinel

Spinel in garnet-spinel lherzolite (YK1923) has the highest Mg# (74.6) and lowest Cr# (25.5) of the dataset (Table 6). Spinels in spinel lherzolite (VR51067) have intermediate Mg# and Cr#. One of the Ca-undersaturated harzburgites has spinels with variable compositions (three grains have Mg# ranging from 57.3 to 69.0 and Cr# from 63.5 to 71.0).

Sulfides

Sulfides are present in several garnet peridotites, mostly as inclusions in olivine, but also in opx and interstitially. They resemble sulfides in olivine xenocrysts described in detail in Aulbach et al. (2004).

Reconstructed whole rocks

Whole-rock compositions were reconstructed from compositions of constituent minerals weighted by primary mineral modes (Table 7). There are no correlations between sample size and mineral modes, suggesting that no bias is introduced due to including relatively small samples in this study.

Garnet harzburgites were not reconstructed because they are too small for a meaningful determination of mineral modes. Garnet lherzolites have mean SiO_2 contents of 44.4 wt%, Cr_2O_3 of 0.5 wt%, Al_2O_3 of 1.2 wt%, FeO of 7.4 wt% and MgO contents of 45.9 wt%. Spinel lherzolite (VR51067) has low FeO (6.3 wt%) and Al_2O_3 (0.5 wt%), and high MgO contents (49.1 wt%).

Geothermobarometry

A combination of two-pyroxene thermometry, Ca-in-opx thermometry (Brey et al. 1990), olivine-garnet thermometry

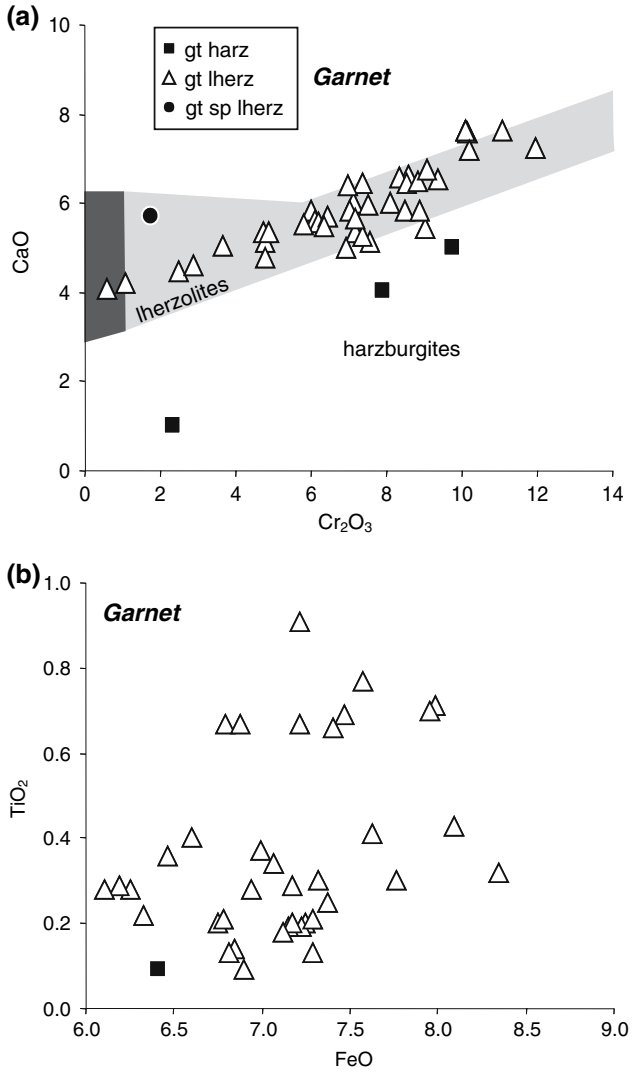

Fig. 2 **a** Cr_2O_3 against CaO and **b** FeO against TiO_2 (wt%) in garnet (highly depleted samples, including two of three garnet harzburgites have TiO_2 contents below the detection limit of 0.06 wt%); *gt* garnet, *sp* spinel, *harz* harzburgite, *lherz* lherzolite; fields in (**a**) after Sobolev et al. (1973) and Gurney (1984)

(O'Neill and Wood 1979) and Al-in-opx barometry (Brey et al. 1990; Nickel and Green 1985) was used to estimate pressure and temperature for the xenoliths, both at assumed pressures (5 GPa for garnet peridotites and 3 GPa for spinel peridotites) and temperatures (1,000°C), as well as by iterative calculations (Table 8). Where applicable, rim compositions were used in the calculations. In accord with previously published results, peridotites in the present study fall on a stepped pressure–temperature array that apparently lies on a 35 mW/m^2 conductive model geotherm to temperatures of ~900°C and on a 40 mW/m^2 geotherm at higher temperatures (not shown), corresponding to the ultradepleted shallow and less depleted deep lithospheric mantle layers beneath Lac De Gras (Pearson et al. 1999; Griffin et al. 1999b). The vast majority of the samples are derived from the deep lithospheric mantle layer. Only a few shallow-layer spinel- or garnet-bearing peridotites have been sampled by the Lac de Gras kimberlites.

Discussion

Melting trends

Melt depletion in the mantle is manifested in refractory compositions and cpx-poor or -absent lithologies that are often interpreted in the context of continental lithosphere formation and craton stabilisation (Boyd and McCallister 1976; Jordan 1988). Mg-numbers in peridotitic olivine from Lac de Gras are for the most part significantly higher than estimates of the Mg# of olivine in fertile mantle (e.g. Norman 1998: 89.4), indicating melt depletion. Despite the uncertainties in the reconstructed whole rock compositions (Table 7), trends among the oxides are evident and merit consideration (cf. MacKenzie and Canil 1999). The negative correlation between MgO and CaO contents (Fig. 3a) and the positive correlation between MgO and NiO contents (Fig. 3b) in reconstructed whole rocks can be interpreted as a partial melting trend, as the residue becomes progressively depleted in CaO and enriched in MgO and NiO (e.g. Herzberg 1999).

Secondary processes

Despite the partial melting trends evident in peridotites from Lac de Gras, original melt depletion signatures may have been corrupted in much of the cratonic SCLM beneath Lac de Gras by secondary processes, as is true for many other peridotite suites (e.g. Gurney and Harte 1980; Menzies and Hawkesworth 1987).

Small amounts of cpx and garnet found in olivine-rich rocks may have exsolved from opx upon cooling (Cox et al. 1987). Most garnet peridotites in the present study are cpx-free on thin-section scale or contain <1 vol.% cpx, which suggests that the cpx that is present is primary. Likewise, the Al_2O_3 contents of depleted peridotites (<4.6 wt%; pyrolite of Ringwood 1975) are correlated with garnet modes that are no higher than those expected for the degree of depletion (Fig. 4), consistent with a primary origin. In contrast, the broad negative correlation of FeO and SiO_2 (Fig. 5), which does not pass through the primitive mantle composition, appears irreconcilable with a simple melt extraction origin, which should lead to a sympathetic behaviour of these mildly incompatible elements (Boyd et al. 1997; Walter 2004, and references therein).

Table 2 Major-element composition of garnet in wt%; *Mg*# is 100Mg/(Mg+Fe), *Cr*# is 100Cr/(Cr+Al); for other abbreviations see Table 1

Sample	Rock type	SiO_2	TiO_2	Al_2O_3	Cr_2O_3	FeO^t	MnO	MgO	CaO	Total	Mg#	Cr#
vr09356	gt lherz	41.13	0.20	18.01	7.17	7.25	0.32	20.10	5.33	99.5	83.2	21.1
vr09358	gt lherz	40.96	0.30	16.27	8.57	7.32	0.26	19.57	6.64	99.9	82.7	26.1
vr09359	gt lherz	40.72	0.19	14.93	10.16	7.23	0.19	18.63	7.59	99.6	82.1	31.3
vr09361	gt lherz	40.18	0.91	13.51	11.06	7.22	0.20	18.22	7.61	98.9	81.8	35.4
vr09364	gt lherz	40.87	0.34	16.89	8.10	7.07	0.31	19.84	6.03	99.5	83.3	24.3
vr09366a	gt lherz	40.75	0.29	16.29	8.36	7.17	0.26	19.38	6.58	99.1	82.8	25.6
vr09370	gt lherz	40.95	0.67	16.43	8.56	6.79	0.29	19.45	6.44	99.6	83.6	25.9
vr09371	gt lherz	40.73	0.19	15.10	10.11	7.15	0.20	18.68	7.61	99.8	82.3	31.0
vr09372a	gt lherz	40.67	0.20	15.07	10.12	7.17	0.22	18.48	7.65	99.6	82.1	31.1
vr19674 pg2	gt lherz	42.83	0.21	22.41	1.07	7.29	0.33	22.16	4.23	100.5	84.4	3.1
vr19674 pg2 rim	gt lherz	42.55	0.24	21.62	2.24	7.40	0.25	21.88	4.49	100.7	84.0	6.5
vr19674 pg3	gt lherz	41.26	<0.06	18.10	7.36	7.94	0.40	18.60	6.45	100.1	80.7	21.4
vr40304	gt lherz	41.04	0.69	16.95	7.12	7.47	0.24	19.51	6.02	99.0	82.3	22.0
vr40332	gt lherz	42.15	0.28	21.36	2.47	6.94	0.24	22.31	4.47	100.2	85.1	7.2
vr40335	gt lherz	42.16	0.43	22.88	0.60	8.09	0.34	21.28	4.09	99.9	82.4	1.7
vr40358	gt lherz	40.69	0.67	13.61	11.96	6.88	0.17	18.60	7.23	99.8	82.8	37.1
vr40358 rim	gt lherz	40.97	0.92	13.80	10.77	7.08	0.20	18.79	7.21	99.7	82.5	34.4
vr40383	gt lherz	42.95	0.36	20.44	3.35	6.82	0.25	21.54	4.65	100.4	84.9	9.9
vr40391	gt lherz	41.92	0.40	17.50	7.57	6.60	0.19	20.93	5.14	100.2	85.0	22.5
vr40391 rim	gt lherz	42.09	0.35	18.01	6.88	6.55	0.21	21.12	5.10	100.3	85.2	20.4
vr43461	gt harz	42.77	<0.06	22.78	2.34	6.74	0.31	24.19	0.99	100.1	86.5	6.4
vr43466	gt lherz	41.43	<0.06	18.64	6.92	7.35	0.34	20.13	5.01	99.8	83.0	19.9
vr43467	gt lherz	40.77	0.67	15.90	8.84	7.22	0.20	19.32	6.50	99.4	82.7	27.2
vr43499	gt lherz	41.63	0.30	19.84	4.77	7.76	0.32	20.01	5.14	99.8	82.1	13.9
vr50851	gt lherz	41.94	0.28	16.54	9.00	6.25	0.17	20.90	5.46	100.5	85.6	26.7
vr50851 rim	gt lherz	41.93	0.29	16.89	8.42	6.07	0.21	20.61	5.72	100.1	85.8	25.1
vr50855	gt lherz	41.59	0.36	17.70	7.35	6.47	0.23	21.14	5.27	100.1	85.3	21.8
vr50861	gt lherz	41.16	<0.06	18.23	6.99	7.65	0.35	18.18	6.41	99.0	80.9	20.5
vr50861 rim	gt lherz	40.95	<0.06	18.21	7.02	8.44	0.50	17.59	6.39	99.1	78.8	20.6
vr50867	gt harz	42.58	0.09	17.38	7.89	6.41	0.15	22.10	4.02	100.6	86.0	23.3
vr50875	gt lherz	41.82	0.18	19.80	4.77	7.12	0.31	20.17	4.80	99.0	83.5	13.9
vr50879	gt lherz	40.98	0.71	17.87	5.99	7.99	0.26	20.08	5.84	99.7	81.8	18.4
vr50882	gt lherz	41.90	0.29	16.73	8.47	6.19	0.15	20.74	5.82	100.3	85.7	25.4
vr50885	gt lherz	41.23	0.28	16.51	8.89	6.11	0.17	20.81	5.84	99.8	85.9	26.5
vr50886	gt lherz	41.04	0.70	18.69	4.73	7.95	0.26	20.06	5.37	98.8	81.8	14.5
vr50904	gt harz	41.17	<0.06	16.18	9.77	7.01	0.25	20.31	4.98	99.7	83.8	28.8
vr50914	gt lherz	41.83	0.14	18.66	6.08	6.84	0.22	20.62	5.62	100.0	84.3	17.9
vr50933	gt lherz	42.32	0.20	18.52	6.19	6.75	0.22	20.97	5.55	100.7	84.7	18.3
vr51902	gt lherz	41.20	0.66	18.40	5.80	7.40	0.23	20.66	5.52	99.9	83.3	17.5
vr51902 rim	gt lherz	40.98	0.67	18.82	5.02	7.29	0.25	20.70	5.36	99.1	83.5	15.2
vr67106	gt lherz	40.83	0.37	15.76	9.35	6.99	0.21	19.09	6.55	99.1	83.0	28.5
vr67112	gt lherz	41.76	0.09	18.68	6.46	6.90	0.22	20.56	5.72	100.4	84.2	18.8
vr67125	gt lherz	40.83	0.21	15.29	10.20	6.78	0.17	18.51	7.18	99.2	83.0	30.9
vr67125 rim	gt lherz	41.04	0.21	15.59	9.68	6.93	0.20	18.75	7.00	99.4	82.8	29.4
yk1912	gt lherz	41.46	0.22	18.07	7.01	6.33	0.20	20.57	5.82	99.7	85.3	20.6
yk1917	gt lherz	41.13	0.32	19.41	4.86	8.35	0.26	20.20	5.37	99.9	81.2	14.4
yk1917 rim	gt lherz	41.07	0.35	19.72	4.58	8.31	0.20	20.13	5.26	99.6	81.2	13.5
yk1919	gt lherz	42.09	0.41	20.74	2.89	7.63	0.27	21.05	4.59	99.7	83.1	8.5

Table 2 continued

Sample	Rock type	SiO_2	TiO_2	Al_2O_3	Cr_2O_3	FeO^t	MnO	MgO	CaO	Total	Mg#	Cr#
yk1919 rim	gt lherz	42.37	0.38	21.23	2.61	7.69	0.25	21.29	4.55	100.4	83.2	7.6
yk1920	gt lherz	41.24	0.25	17.40	7.52	7.37	0.25	19.99	5.97	100.0	82.9	22.5
yk1923	gt sp lherz	42.02	<0.06	22.61	1.75	8.41	0.32	19.37	5.68	100.2	80.4	4.9
yk1938	gt lherz	41.70	<0.06	21.32	3.68	7.88	0.36	20.23	5.04	100.2	82.1	10.4
yk2471	gt lherz	41.74	0.13	18.72	6.33	6.81	0.22	20.62	5.50	100.1	84.4	18.5
yk2472	gt lherz	40.58	0.77	15.46	9.07	7.57	0.21	19.05	6.77	99.5	81.8	28.2
yk2472 rim	gt lherz	40.86	0.75	15.86	8.61	7.52	0.20	19.17	6.62	99.6	82.0	26.7
yk2474	gt lherz	41.80	0.13	17.97	7.15	7.29	0.25	20.03	5.64	100.2	83.0	21.1

Table 3 Major-element composition of clinopyroxene in wt%; inhomo = inhomogeneous; for other abbreviations see Tables 1 and 2

Sample	Comment	Rock type	SiO_2	TiO_2	Al_2O_3	Cr_2O_3	FeO^t	MgO	CaO	Na_2O	Total	Mg#
vr09359		gt lherz	55.10	<0.06	0.61	0.86	2.62	19.31	21.12	0.52	100.1	92.9
vr09361		gt lherz	54.89	0.19	1.25	2.05	2.74	18.10	18.73	1.58	99.5	92.2
vr09370		gt lherz	54.87	0.27	1.76	2.70	2.09	16.58	19.14	2.21	99.6	93.4
vr19674 pg2		gt lherz	55.56	0.07	1.75	0.59	2.75	18.55	19.54	1.22	100.0	92.3
vr19674 pg3		gt lherz	55.18	<0.06	1.48	1.67	1.42	16.52	22.08	1.44	99.8	95.4
vr40304		gt lherz	54.70	0.21	1.39	1.29	3.02	18.29	18.95	1.39	99.2	91.5
vr40332		gt lherz	54.85	0.09	1.77	1.18	2.53	18.33	19.33	1.45	99.5	92.8
vr40335		gt lherz	54.87	0.31	2.41	0.33	2.62	17.06	20.07	1.75	99.4	92.1
vr43467		gt lherz	54.86	0.20	1.36	1.66	2.85	18.45	18.82	1.54	99.7	92.0
vr43499	inhomo Ca	gt lherz	54.87	0.15	1.54	1.68	2.32	17.26	20.17	1.66	99.7	93.0
vr50861		gt lherz	55.23	<0.06	1.60	2.03	1.34	15.95	21.42	1.55	99.1	95.5
vr50875		gt lherz	54.91	0.07	2.20	1.94	2.43	16.27	19.01	2.07	98.9	92.3
vr50879		gt lherz	54.76	0.19	1.43	1.29	3.18	18.26	18.98	1.31	99.4	91.1
vr50886		gt lherz	54.13	0.22	1.48	1.10	3.36	18.27	18.66	1.31	98.5	90.6
vr50914		gt lherz	55.34	<0.06	1.20	1.08	2.53	18.66	19.96	1.01	99.8	92.9
vr50933		gt lherz	56.05	<0.06	1.39	1.28	2.46	18.64	19.63	1.20	100.7	93.1
vr51067		sp lherz	54.76	0.47	2.27	1.16	1.39	16.69	22.72	1.16	100.6	95.5
vr51902		gt lherz	54.77	0.21	1.62	1.15	3.33	18.80	18.38	1.48	99.7	95.8
vr67112		gt lherz	55.13	<0.06	1.08	1.05	2.44	18.84	20.38	0.87	99.8	93.2
vr67112	rim	gt lherz	55.01	<0.06	0.95	1.04	2.44	18.67	20.89	0.84	99.8	93.2
vr67112b2		gt lherz	54.69	<0.06	1.07	1.04	2.55	18.57	20.40	0.87	99.2	92.8
vr67125		gt lherz	54.97	<0.06	0.83	1.23	2.49	18.65	20.30	0.90	99.4	93.0
yk1917		gt lherz	54.96	0.10	1.41	1.09	3.17	18.01	19.72	1.34	99.8	91.0
yk1919		gt lherz	55.13	0.13	2.14	0.89	3.04	17.93	18.43	1.78	99.5	91.3
yk1919	rim	gt lherz	55.09	0.16	2.04	0.88	3.14	17.88	19.02	1.64	99.8	91.0
yk1920		gt lherz	54.88	0.08	1.42	1.55	2.83	18.19	18.99	1.53	99.5	92.0
yk1923	inhomo Al	gt sp lherz	54.44	<0.06	1.68	0.67	1.52	16.89	24.00	0.65	99.8	95.2
yk2471		gt lherz	55.13	<0.06	1.42	1.39	2.44	18.38	19.70	1.32	99.8	93.1
yk2472		gt lherz	54.78	0.16	1.15	1.72	2.78	18.34	19.13	1.45	99.5	92.2
yk2472	rim	gt lherz	54.51	0.28	0.51	1.68	2.89	17.95	21.19	1.02	100.0	91.7
yk2474		gt lherz	55.68	<0.06	1.75	2.29	2.31	16.90	19.46	1.98	100.4	92.9

If the moderately silica-rich, Fe-poor peridotites formed by a physical process involving sorting of olivine (high FeO and low SiO_2) and opx (low FeO and high SiO_2) (Boyd 1997), they should lie on a mixing line between olivine and opx. However, this is not observed for our samples, where the distance between the mixing line and

Table 4 Major-element composition of orthopyroxene in wt%; for abbreviations see Tables 1 and 2

Sample	Rock type	SiO_2	TiO_2	Al_2O_3	Cr_2O_3	FeO^t	MnO	MgO	CaO	NiO	Na_2O	Total	Mg#
vr09356	gt lherz	58.21	<0.06	0.48	0.33	4.80	0.10	36.09	0.46	0.10	0.14	100.7	93.1
vr09358	gt lherz	57.97	<0.06	0.53	0.35	5.05	0.13	35.56	0.80	0.12	0.11	100.6	92.6
vr09359	gt lherz	58.16	<0.06	0.45	0.31	5.04	0.12	35.74	0.86	0.12	0.05	100.9	92.7
vr09361	gt lherz	57.77	<0.06	0.53	0.47	5.01	0.14	35.47	0.79	0.13	0.16	100.5	92.7
vr09366	gt lherz	57.61	<0.06	0.53	0.34	4.91	0.13	35.45	0.82	0.12	0.10	100.1	92.8
vr09370	gt lherz	58.29	<0.06	0.49	0.38	4.29	0.10	36.40	0.50	0.11	0.13	100.7	93.8
vr09371	gt lherz	58.09	<0.06	0.45	0.30	4.97	0.13	35.64	0.84	0.13	0.05	100.6	92.7
vr09372	gt lherz	58.06	<0.06	0.46	0.33	5.13	0.10	35.85	0.81	0.11	0.05	100.9	92.6
vr19674 pg3	gt lherz	58.66	<0.06	0.42	0.22	4.42	0.12	36.88	0.21	0.08	0.04	101.1	93.7
vr40304	gt lherz	57.56	0.13	0.56	0.32	5.35	0.15	35.04	0.84	0.13	0.15	100.2	92.1
vr40332	gt lherz	57.71	<0.06	0.60	0.22	4.84	0.10	35.92	0.74	0.11	0.14	100.4	93.0
vr40335	gt lherz	57.95	0.13	0.53	0.04	5.39	0.10	35.57	0.48	0.10	0.11	100.4	92.2
vr40358	gt lherz	58.67	0.12	0.53	0.45	4.88	0.12	35.50	0.81	0.13	0.17	101.4	92.8
vr40391	gt lherz	59.02	<0.06	0.53	0.33	4.46	0.11	36.24	0.60	0.12	0.11	101.6	93.5
vr43466	gt lherz	58.36	<0.06	0.36	0.22	4.37	0.11	36.64	0.29	0.10	0.04	100.5	93.7
vr43467	gt lherz	57.70	0.12	0.57	0.38	5.08	0.12	35.39	0.81	0.12	0.18	100.5	92.6
vr43499	gt lherz	58.30	0.07	0.46	0.22	5.15	0.12	35.87	0.45	0.10	0.10	100.9	92.5
vr50851	gt lherz	59.07	<0.06	0.58	0.43	4.25	0.12	36.13	0.69	0.12	0.17	101.6	93.8
vr50855	gt lherz	58.14	<0.06	0.52	0.34	4.45	0.11	36.09	0.61	0.12	0.11	100.5	93.5
vr50861	gt lherz	58.32	<0.06	0.37	0.18	4.74	0.12	35.39	0.28	<0.08	0.04	99.5	93.0
vr50875	gt lherz	57.92	<0.06	0.56	0.26	4.78	0.12	35.09	0.52	0.11	0.14	99.5	92.9
vr50879	gt lherz	57.57	<0.06	0.61	0.30	5.63	0.13	34.78	0.84	0.11	0.13	100.1	91.7
vr50885	gt lherz	58.00	<0.06	0.56	0.43	4.18	0.10	35.76	0.68	0.10	0.17	100.0	93.9
vr50886	gt lherz	57.19	<0.06	0.67	0.28	5.86	0.13	34.27	0.95	0.14	0.17	99.7	91.2
vr50904	gt harz	58.53	<0.06	0.37	0.27	4.43	0.10	36.22	0.29	0.10	<0.04	100.4	93.6
vr50914	gt lherz	58.36	<0.06	0.53	0.26	4.90	0.12	35.76	0.77	0.13	0.10	100.9	92.9
vr51067	sp lherz	58.02	0.16	1.34	0.35	4.54	0.11	35.80	0.36	<0.08	<0.04	100.8	93.4
vr51902	gt lherz	57.45	0.12	0.67	0.28	5.47	0.13	35.04	0.91	0.13	0.18	100.4	93.9
vr67106	gt lherz	58.00	<0.06	0.56	0.40	4.88	0.10	35.30	0.76	0.13	0.16	100.3	92.8
vr67112	gt lherz	58.11	<0.06	0.51	0.26	4.88	0.12	36.01	0.77	0.12	0.09	100.9	92.9
vr67112b2	gt lherz	57.72	<0.06	0.52	0.25	4.92	0.10	35.55	0.76	0.11	0.10	100.0	92.8
vr67125	gt lherz	58.10	<0.06	0.51	0.36	4.76	0.12	35.41	0.80	0.12	0.10	100.3	93.0
yk1912	gt lherz	58.06	<0.06	0.51	0.30	4.35	0.10	36.28	0.68	0.11	0.10	100.5	93.7
yk1917	gt lherz	57.47	<0.06	0.59	0.24	5.85	0.11	34.70	0.76	0.13	0.13	100.0	91.4
yk1919	gt lherz	57.75	0.07	0.69	0.20	5.42	0.12	34.83	0.76	<0.08	0.19	100.1	92.0
yk1920	gt lherz	57.87	<0.06	0.60	0.34	5.10	0.11	35.39	0.77	0.12	0.17	100.5	92.5
yk1923	gt sp lherz	57.68	<0.06	1.10	0.30	4.80	<0.09	35.80	0.29	<0.08	<0.04	100.1	93.0
yk1938	gt lherz	58.23	<0.06	0.48	0.24	4.43	0.09	36.75	0.34	0.09	0.04	100.7	93.7
yk2471	gt lherz	58.16	<0.06	0.56	0.30	4.74	0.11	35.79	0.75	0.12	0.14	100.7	93.1
yk2472	gt lherz	57.79	0.10	0.54	0.37	5.25	0.12	35.32	0.80	0.13	0.16	100.6	92.3
yk2474	gt lherz	58.72	<0.06	0.52	0.33	4.85	0.11	35.77	0.53	0.10	0.14	101.1	92.9

the data trend apparently increases with increasing SiO_2 content (though not outside the uncertainty of the reconstructed whole rock compositions; Fig. 6a). If opx-rich peridotites in our study had formed by reaction with Si-rich melts (Boyd 1997; Kelemen et al. 1998), a positive correlation between NiO in olivine and modal opx would be expected (Boyd 1997). This correlation also is not observed in our dataset (Fig. 6b), although two of the samples with the highest silica content (VR09361, YK1938) have olivines with high NiO contents (>0.4 wt%).

Moderately silica-rich, Fe-poor rocks can be produced by peritectic production of opx on the solidus, with higher

Table 5 Major-element composition of olivine in wt%; for abbreviations see Tables 1 and 2

Sample	Rock type	SiO_2	FeO^t	MnO	MgO	NiO	Total	Mg#
vr09356	gt lherz	41.00	8.08	0.10	51.13	0.36	100.7	91.9
vr09358	gt lherz	40.93	8.43	0.11	50.61	0.39	100.5	91.5
vr09359	gt lherz	41.12	8.41	0.11	50.84	0.39	100.9	91.5
vr09361	gt lherz	40.98	8.37	0.12	50.69	0.40	100.6	91.5
vr09364	gt lherz	41.04	7.56	0.11	51.61	0.37	100.7	92.4
vr09366	gt lherz	40.77	8.26	0.11	50.72	0.42	100.3	91.6
vr09370	gt lherz	41.26	7.17	0.11	51.90	0.30	100.7	92.8
vr09371	gt lherz	41.07	8.36	0.11	50.71	0.41	100.7	91.5
vr09372	gt lherz	41.11	8.36	0.10	50.96	0.38	100.9	91.6
vr19674 pg2	gt lherz	41.06	8.72	0.10	50.65	0.40	100.9	91.2
vr19674 pg3	gt lherz	41.40	7.22	<0.09	51.90	0.40	100.9	92.8
vr40304	gt lherz	40.79	8.83	0.15	50.03	0.43	100.2	91.0
vr40332	gt lherz	40.79	8.09	0.10	51.22	0.38	100.6	91.9
vr40335	gt lherz	41.05	9.12	0.12	50.21	0.35	100.9	90.8
vr40358	gt lherz	41.69	8.14	0.11	51.07	0.42	101.4	91.8
vr40391	gt lherz	41.85	7.49	0.09	51.55	0.38	101.4	92.5
vr43466	gt lherz	41.20	7.19	0.09	51.56	0.37	100.4	92.7
vr43467	gt lherz	40.95	8.45	0.11	50.50	0.38	100.4	91.4
vr43499	gt lherz	41.17	8.61	0.11	50.68	0.35	100.9	91.3
vr50851	gt lherz	41.92	7.09	0.09	51.92	0.36	101.4	92.9
vr50855	gt lherz	40.92	7.50	0.10	51.47	0.39	100.4	92.4
vr50861	gt lherz	41.40	7.59	0.10	50.16	0.36	99.6	92.2
vr50875	gt lherz	41.12	8.19	0.10	49.88	0.36	99.7	91.6
vr50879	gt lherz	40.50	9.42	0.13	49.49	0.35	99.9	90.4
vr50885	gt lherz	40.94	6.94	0.09	51.44	0.36	99.8	93.0
vr50886	gt lherz	40.58	9.84	0.12	49.02	0.41	100.0	89.9
vr50904	gt harz	41.23	7.43	0.11	51.17	0.36	100.3	92.5
vr50914	gt lherz	41.15	8.21	0.12	50.91	0.41	100.8	91.7
vr51067	sp lherz	41.79	6.58	0.10	52.06	0.35	100.9	93.4
vr51902	gt lherz	40.66	8.91	0.11	50.45	0.38	100.5	91.0
vr67106	gt lherz	41.15	8.17	0.11	50.51	0.41	100.3	91.7
vr67112	gt lherz	41.01	8.21	0.11	51.11	0.37	100.8	91.7
vr67112b2	gt lherz	40.99	8.25	0.12	50.66	0.40	100.4	91.6
vr67125	gt lherz	41.09	8.17	0.11	50.41	0.39	100.2	91.7
yk1912	gt lherz	41.16	7.34	0.09	51.55	0.37	100.5	92.6
yk1917	gt lherz	40.31	9.87	0.10	49.12	0.39	99.8	89.9
yk1919	gt lherz	40.94	9.09	0.10	49.95	0.38	100.5	90.7
yk1919 rim	gt lherz	40.28	9.05	<0.09	49.39	0.39	99.1	90.7
yk1920	gt lherz	40.88	8.53	0.12	50.64	0.38	100.5	91.4
yk1923	gt sp lherz	41.49	7.03	<0.09	51.52	0.53	100.6	92.9
yk1938	gt lherz	41.23	7.01	<0.09	52.11	0.40	100.8	93.0
yk1938 rim	gt lherz	40.79	9.05	0.14	50.25	0.30	100.5	90.8
yk2471	gt lherz	41.20	7.96	0.11	51.13	0.38	100.8	92.0
yk2472	gt lherz	40.87	8.71	0.12	50.51	0.39	100.6	91.2
yk2474	gt lherz	41.50	8.21	0.10	50.81	0.35	101.0	91.7

degrees of partial melting required at higher pressures for the reaction to occur (Walter 1998 and references therein). These high degrees of partial melting may well have been achieved in the hotter Archaean Earth, especially in plumes (Nisbet et al. 1993). Unlike peridotites from the Kaapvaal craton, peridotites from Lac de Gras have relatively low

Table 6 Major-element composition of spinel in wt%; Fe^{3+} # = $100Fe^{3+}/(Fe^{3+} + Fe^{2+})$, Fe^{3+} calculated from stoichiometry after Droop (1987); FeO^{recalc} and $Fe_2O_3^{calc}$ refer to contents (re)calculated from total FeO; comments: *type* refers to different compositions in inhomogeneous spinels; *incl* = included; for other abbreviations see Tables 1 and 2

Sample	Comment	Rock type	SiO_2	TiO_2	Al_2O_3	Cr_2O_3	FeO^{recalc}	$Fe_2O_3^{calc}$	MnO	MgO	NiO	ZnO	V_2O_5	Total	Mg#	Cr#	Fe^{3+}#
vr19674 pg3		gt lherz	<0.07	<0.06	8.45	61.26	16.43	1.77	<0.09	10.82	<0.08	na	na	98.7	51.7	82.9	8.8
vr43461	Type1	gt harz	0.14	<0.06	18.83	48.74	11.85	3.77	0.23	14.78	0.13	0.07	0.38	98.9	63.4	63.5	22.3
vr43461	Type2	gt harz	0.11	<0.06	20.60	46.94	11.38	4.15	0.21	15.35	0.11	0.09	0.38	99.3	64.4	60.4	24.7
vr43461	Type3	gt harz	0.13	<0.06	22.59	45.18	11.36	3.79	0.17	15.61	0.14	0.07	0.33	99.4	65.3	57.3	23.1
vr43461	Incl	gt harz	0.11	<0.06	19.01	48.08	11.71	4.07	0.24	14.83	0.13	<0.06	0.40	98.6	63.2	62.9	23.8
vr51067		sp lherz	<0.07	0.22	24.29	43.82	15.69	1.79	0.26	12.85	<0.08	0.31	0.17	99.4	57.0	54.8	9.3
vr51067	Rim	sp lherz	<0.07	0.16	24.18	43.36	13.94	2.61	0.25	13.82	<0.08	0.34	0.18	98.8	60.2	54.6	14.4
vr67106	Type1	gt lherz	0.19	0.60	33.03	29.90	12.58	6.62	0.35	16.28	<0.08	<0.06	0.13	99.7	61.0	37.8	32.2
vr67106	Type2	gt lherz	0.16	2.97	9.85	48.29	15.07	7.35	0.28	13.23	0.11	0.12	0.29	97.7	52.1	76.7	30.5
yk1920		gt lherz	0.38	2.29	9.27	49.91	15.04	6.84	0.36	12.85	0.12	0.10	0.24	97.4	51.9	78.4	29.0
yk1923		gt sp lherz	<0.07	0.09	45.15	23.01	9.13	2.94	<0.09	19.39	0.31	0.20	0.10	100.3	74.6	25.5	22.4
yk1923	Type1 incl	gt sp lherz	<0.07	0.11	34.02	33.72	11.56	2.87	0.12	16.51	0.21	0.20	0.15	99.5	67.5	39.9	18.2
yk1923	Type2 incl	gt sp lherz	<0.07	0.20	26.93	39.97	12.97	3.27	0.17	14.76	0.18	0.27	0.17	98.9	62.3	49.9	18.5
yk2472		gt lherz	0.10	2.56	6.88	52.04	15.79	8.36	0.35	12.21	0.13	0.10	0.20	98.7	48.2	84.5	31.9

opx/ol (Pearson et al. 1999) and the moderate opx enrichment in most samples may have a primary origin.

Samples at the other end of the spectrum, with low SiO_2 yet relatively high FeO, may have formed by reaction with silica-undersaturated melts, a process that would lead to opx dissolution and an increase in modal olivine (Griffin et al. 1999a). Olivine enrichment may also be achieved by fractional crystallisation of olivine upon cooling and decompression of magmas that were produced deeper in the melt column and percolated into the depleted mantle (Kinzler and Grove 1999). Either mechanism amounts to a secondary process entailing FeO enrichment. Two samples (VR43467, YK2472) with high FeO contents (>8 wt%) contain garnets with high TiO_2 contents (0.67 and 0.87 wt%, respectively), which may point to interaction with mafic melts leading to concomitant enrichment in FeO and TiO_2 (e.g. Smith and Boyd 1987).

Secondary enrichment of the lithospheric mantle in FeO is supported by the compositions of olivine inclusions in diamonds from the same area (Davies et al. 1999), which have higher average Mg-numbers (92.6) than olivine in peridotites (91.7) (Fig. 7). Diamond growth and entrapment of inclusions predates kimberlite magmatism, often by billions of years (Shirey et al. 2004 and references therein). Inclusions in diamonds from the Panda kimberlite, just north of Lac de Gras, were dated at ~3.5 Ga (Westerlund et al. 2006). In contrast, entrained xenoliths reflect a snapshot of mantle composition at the time of emplacement, which is Eocene in the case of the Lac de Gras kimberlites. Higher average FeO contents in the xenolithic olivine suggest a secular evolution towards more fertile compositions through metasomatic processes. While these effects are evident in peridotites with contents of incompatible major elements that exceed those of primitive mantle, they may have also cryptically affected peridotites with overall depleted signatures, where they are not easily recognised.

Plume subcretion or lithosphere accretion?

The evidence for lithosphere accretion

It has been argued that high Cr_2O_3 contents and Cr/Al observed in some garnets from highly depleted source rocks require depletion at shallow levels (spinel stability field). At low pressures, the bulk distribution coefficient for Cr, which is controlled by spinel and orthopyroxene, is significantly higher than that for Al, whereas at higher pressures Cr and Al are not significantly fractionated (Stachel et al. 1998, 2003; Canil 2004).

In our sample suite, Cr and Al oxides are broadly positively correlated (Fig. 8), a feature that is observed in other Archean xenolith suites, but not in younger ones, nor in residues of high-degree melting at shallow depths

Table 7 Whole-rock compositions reconstructed from modal data and mineral compositions; uncertainties (absolute errors) based on modal uncertainties calculated after Solomon (1963); for abbreviations see Tables 1 and 2

Sample	Rock type	SiO_2	2 σ	Al_2O_3	2 σ	Cr_2O_3	2 σ	FeO^t	2 σ	MgO	2σ	CaO	2σ	NiO	2σ	Total
vr09361	gt lherz	47.7	13.4	1.2	1.6	1.1	1.3	6.8	1.5	41.5	8.3	1.6	3.1	0.26	0.05	100.4
vr09371	gt lherz	42.9	5.4	0.7	1.1	0.5	0.7	7.9	0.9	47.8	4.9	0.4	0.6	0.37	0.04	100.7
vr43466	gt lherz	43.8	2.6	0.8	1.0	0.3	0.4	6.8	0.4	48.1	1.6	0.3	0.3	0.31	0.01	100.5
vr43467	gt lherz	41.8	7.2	0.4	0.9	0.3	0.5	8.3	0.8	49.1	4.5	0.2	0.4	0.36	0.02	100.6
vr50851	gt lherz	45.0	3.2	1.1	1.0	0.7	0.6	6.5	0.4	47.2	1.8	0.5	0.4	0.30	0.01	101.5
vr50861	gt lherz	43.2	8.8	1.2	0.8	0.5	0.4	7.2	0.4	46.4	3.0	0.6	3.2	0.31	0.01	99.6
vr50914	gt lherz	45.1	8.4	1.2	1.6	0.5	0.6	7.3	0.8	45.4	4.1	0.7	2.6	0.32	0.02	100.8
vr51067	sp lherz	44.0	3.0	0.5	0.1	0.5	0.02	6.3	0.3	49.1	2.1	0.1	0.02	0.30	0.01	100.9
vr67106	gt lherz	42.8	5.0	0.4	1.5	0.3	0.9	7.8	0.7	48.4	2.7	0.2	0.6	0.37	0.01	100.5
vr67112	gt lherz	45.3	8.2	0.1	0.2	0.1	0.1	7.3	0.6	47.1	3.9	0.4	2.9	0.31	0.02	100.9
vr67125	gt lherz	45.9	5.2	0.6	1.2	0.5	0.8	7.1	0.7	44.6	3.2	1.1	1.2	0.30	0.02	100.3
yk1912	gt lherz	43.9	10.2	2.8	4.1	1.1	1.6	6.7	1.6	44.5	6.6	1.0	1.3	0.28	0.03	100.5
yk1917	gt lherz	44.3	13.0	0.9	2.8	0.3	0.7	8.9	1.7	44.5	7.2	0.6	3.9	0.31	0.05	100.0
yk1920	gt lherz	43.5	9.4	1.5	2.5	0.7	1.1	7.8	1.4	45.2	6.3	1.2	1.8	0.31	0.04	100.6
yk1938	gt lherz	46.6	3.1	3.1	0.9	0.6	0.1	6.3	0.4	42.9	2.5	0.8	0.2	0.25	0.02	100.7
yk2471	gt lherz	44.1	9.0	1.8	1.5	0.7	0.5	7.3	0.8	45.6	4.5	0.8	2.8	0.30	0.02	100.8
yk2472	gt lherz	43.9	4.2	0.6	0.8	0.4	0.5	8.1	0.7	46.8	3.4	0.4	0.4	0.33	0.02	100.7
yk2474	gt lherz	44.6	10.8	1.4	2.4	0.6	1.0	7.5	1.2	45.8	5.8	0.7	2.6	0.28	0.03	101.0

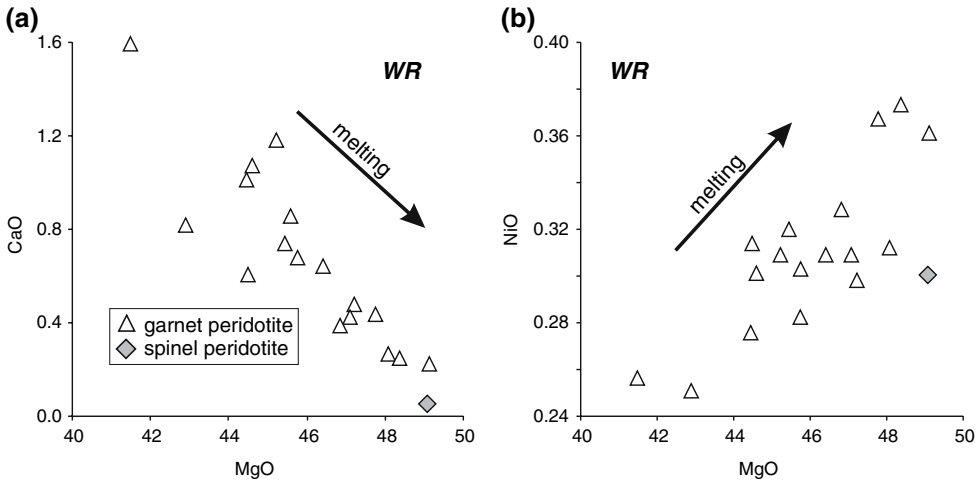

Fig. 3 MgO against **a** CaO and **b** NiO (wt%) in reconstructed peridotites; qualitative partial melting trends are also shown

(Griffin et al. 1999a). The positive correlation suggests that both garnet and spinel were exhausted from the residue during high degrees of partial melting. Above 4–5 GPa and below 7 GPa, i.e. at conditions corresponding to the pressures of last equilibration of most peridotites in the sample suite (Table 8), cpx is the first phase consumed during partial melting of fertile peridotite, followed by garnet, while olivine and a Ca- and Al-rich opx remain on the solidus (Canil 1992; Walter 2004). Upon cooling, garnet and cpx exsolve from aluminous opx (Cox et al. 1987; Canil 1991).

In batch melting experiments at 6 GPa and 1,770°C, with olivine plus opx in the residue, olivine has Cr_2O_3 contents of ~0.24 wt% and a similar amount of Al_2O_3, but it represents ~67% of the volume of the residue (Walter 2004). The resulting bulk $D_{Cr/Al}^{residue/melt}$ is around 7 and the bulk residue contains 0.34 wt% Cr_2O_3 and 1.46 wt% Al_2O_3. Orthopyroxene in our samples has three times lower Cr_2O_3 contents (0.3 wt%) than experimental high-temperature opx (0.9 wt%), and olivine generally has Cr_2O_3 below the detection limit (0.08 wt%) compared to 0.24 wt% in the experiments. This suggests that upon cooling and subsolidus re-equilibration, virtually all Cr_2O_3 in olivine and two thirds of the Cr_2O_3 in high-temperature opx is redistributed to cpx and garnet exsolving from the opx. This can only account for ~80% of the average Cr_2O_3

Table 8 Temperatures and pressures (T_{BKN}, $T_{Ca\text{-}in\text{-}opx}$, P_{BKN}: Brey et al. 1990; T_{OW79}: O'Neill and Wood 1979; P_{NG}: Nickel and Green 1985) calculated at assumed pressures of 5 GPa (except spinel peridotite: 3 GPa) and temperatures of 1000° C, and solved simultaneously

Sample	Preset P and T					Simultaneous solutions					
	T_{BKN}	T_{OW79}	$T_{Ca\text{-}in\text{-}opx}$	P_{BKN}	P_{NG}	T_{BKN} @P_{BKN}	P_{BKN} @T_{BKN}	T_{OW79} @P_{NG}	P_{NG} @T_{OW79}	$T_{Ca\text{-}in\text{-}opx}$ @P_{BKN}	P_{BKN} @$T_{Ca\text{-}in\text{-}opx}$
vr09356		1,057		43	48			1,061	51		
vr09358		1,092		43	49			1,106	53		
vr09359	1,166	1,076	1,186	47	54	1,179	57	1,110	59	1,234	60
vr09361	1,220	1,066	1,163	46	53	1,237	59	1,094	57	1,194	56
vr09364		1,004									
vr09366		1,081		44	49			1,094	53		
vr09370	1,098	983	1,051	49	54	1,107	55	998	53	1,061	52
vr09371		1,088		48	54			1,123	59		
vr09372		1,071		48	55			1,106	59		
vr19674 pg3	809	834	879	49	52	789	35	796	41	830	37
vr40302	1,081		1,019								
vr40304	1,217	1,111	1,182	44	48	1,239	60	1,131	55	1,230	60
vr40332	1,193	1,176	1,148	43	45	1,207	57	1,202	56	1,167	54
vr40335	1,067	1,089	1,041	48	47	1,072	53	1,106	54	1,045	51
vr40358		1,061		44	53			1,085	56		
vr40391		1,109		45	49			1,134	56		
vr43466		912		53	55			914	50		
vr43467	1,220	1,096	1,171	42	48	1,230	55	1,106	52	1,181	52
vr43499	1,070	1,036	1,027	49	50	1,078	54	1,047	53	1,031	51
vr50851		1,121		41	46			1,130	52		
vr50855		1,131		45	49			1,163	58		
vr50861	893	813	935	52	53	882	43	775	42	916	45
vr50867		1,115		44	50			1,148	58		
vr50875	1,121	1,092	1,062	43	45	1,123	51	1,092	50	1,040	45
vr50879	1,222	1,139	1,182	44	47	1,247	62	1,161	55	1,237	61
vr50882		1,192		42	47			1,221	58		
vr50885		1,112		41	47			1,123	52		
vr50886	1,246	1,170	1,218	41	44	1,269	61	1,185	54	1,275	61
vr50904		1,000		49	56			1,033	58		
vr50914	1,199	1,170	1,156	45	47	1,217	59	1,201	58	1,192	57
vr50933	1,218	1,170	1,156	42	45	1,230	56	1,190	55	1,166	52
vr51067	791		920								
vr51902	1,253	1,186	1,204	41	44	1,271	59	1,202	54	1,235	56
vr67106		1,088	1,154	40	47			1,091	51	1,145	48
vr67112	1,143	1,146	1,157	44	48	1,150	54	1,172	56	1,187	56
vr67112b2	1,170		1,155								
vr67125	1,178	1,093	1,169	44	50	1,184	53	1,111	55	1,185	53
yk1912		1,117		45	49			1,142	56		
yk1917	1,166	1,140	1,156	42	44	1,176	55	1,151	53	1,181	55
yk1919	1,199	1,173	1,173	47	47	1,226	63	1,213	60	1,245	65
yk1920	1,205	1,100	1,159	39	45	1,210	52	1,096	49	1,153	49
yk1923	602	697	857	39	38	586	16	639	19	858	30
yk1938		840		51	51			782	38		
yk2471	1,184	1,126	1,151	41	45	1,190	53	1,132	52	1,155	51
yk2472	1,072	1,079	1,168	43	49	1,066	47	1,091	53	1,192	55
yk2474	1,118	1,064	1,062	42	46	1,117	49	1,062	49	1,035	44

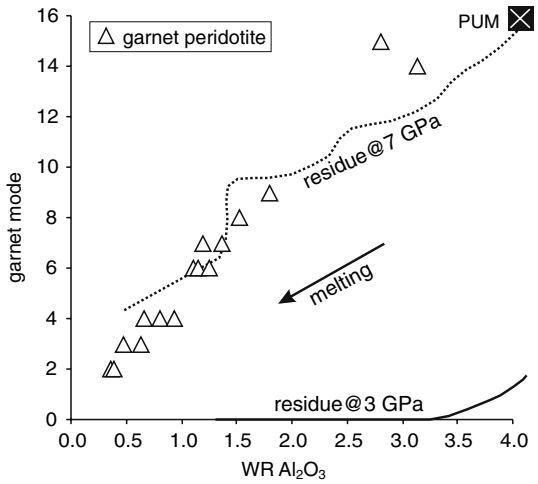

Fig. 4 Al_2O_3 contents (wt%) of reconstructed whole rocks against garnet modes (vol.%). Partial melting trends for melting at 7 and 3 GPa, using a primitive upper mantle (*PUM*) starting material, are taken from Canil (2004). At 3 GPa, garnet is consumed after about 10% melting, corresponding to Al_2O_3 contents of about 3.5 wt% (Canil 2004)

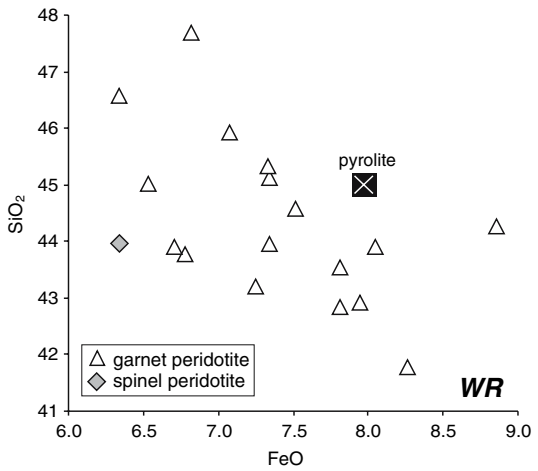

Fig. 5 FeO against SiO_2 (wt%) in reconstructed whole rocks; primitive mantle composition (pyrolite; Ringwood 1975) is shown for reference

content in peridotitic garnet and cpx from Lac de Gras. Also, the Cr_2O_3/Al_2O_3 of the experimental residue is 0.23, whereas average garnet lherzolites from Lac de Gras have a higher Cr_2O_3/Al_2O_3 of 0.5. This discrepancy may be alleviated if higher degrees of batch melting are invoked. However, in the absence of experimental confirmation of this possibility, available evidence suggests that shallow depletion, in the spinel stability field, is required for formation of high-Cr/Al peridotite (Fig. 8 in Canil, 2004). If, on the other hand, the inference of high-pressure melting in the absence of an aluminous phase is correct, it may indicate that garnet with Cr# as high as 30, as observed in our sample suite, can exsolve from such residues upon cooling.

Some arguments regarding depth of melting have focused on the different geochemical signatures that are imposed during melting with residual garnet ± cpx (garnet stability field) as opposed to residual cpx (spinel stability field). The abundances of mildly incompatible elements in peridotites appear to be incompatible with the presence of garnet in the residue and hence have been used as evidence for a shallow origin (Kelemen et al. 1998; Canil 2004). However, arguments based on the presence of residual cpx versus garnet do not hold if the degree of partial melting and melting conditions were such that neither remained on the solidus (e.g. Griffin et al. 1999a).

At temperatures near or above the mantle solidus and pressures ≤ 6 GPa, appropriate to melting in an ascending mantle plume, garnet and cpx are dissolved in a Ca- and Al-rich opx (Canil 1992). This Ca- and Al-rich opx might have partitioning characteristics similar to cpx, thus explaining the ''cpx-signature'' observed in depleted peridotites (Canil 2004).

The evidence for plume subcretion

Melting experiments have shown that residues from melting at low pressures have higher FeO-contents than residues generated at high pressures and that low FeO can only be produced during high-pressure melting extraction. This observation makes the low FeO contents of most cratonic peridotites (Griffin et al. 1999b) the single most important feature in support of a high-pressure origin. Olivine in the majority of samples (n = 35) from Lac de Gras has Mg# ≤ 92, which would be consistent with 25–38% partial melt extraction at pressures <3 GPa, corresponding to an oceanic setting (Herzberg 1999). Olivines in 18 peridotites have Mg# > 92, which indicates 38–50% partial melting at 6–3 GPa, corresponding to a plume setting (Herzberg 1999).

The degree and depth of melt depletion experienced by the SCLM beneath the central Slave Craton may also be assessed by comparing the contents of major element oxides in reconstructed whole rocks with those of experimental melting residues (Fig. 9). The conclusions that can be drawn from this exercise are tempered by the large uncertainties associated with whole-rock compositions reconstructed from small samples with large grain sizes. Bearing this in mind, most samples in our study have higher MgO contents at a given FeO content than those from other localities in the Slave Craton (Torrie, MacKenzie and Canil 1999; Jericho, Kopylova et al. 1999; Gahcho Kué, Kopylova and Caro 2004), consistent with distinct origins and extended metasomatic histories for these lithosphere sections.

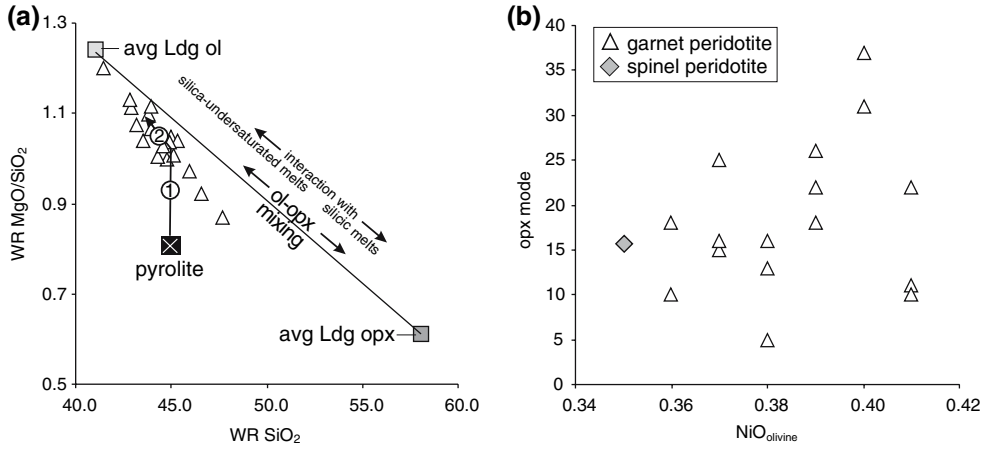

Fig. 6 **a** Whole-rock SiO_2 (wt%) against MgO/SiO_2. A mixing line between average olivine and opx from Lac de Gras (*LdG*) is also shown, along with a primitive mantle composition (pyrolite; Ringwood 1975) and a qualitative melting trend that comprises (1) peritectic opx formation on the solidus, followed by (2) infusion of olivine by crystallization from deeper melt batches ascending through the residue (Kinzler and Grove 1999), as well as trends for enrichment of depleted peridotites by silica-undersaturated and silicic melts, respectively. **b** NiO (wt%) in olivine against opx mode

All but four garnet peridotites have been entrained by the host kimberlite from depths corresponding to 4.2–5.8 GPa (Table 8). Considering the large uncertainties of reconstructed whole-rock compositions, there is good coincidence of the calculated pressures of last equilibration and pressures of equilibrium melting (~4 to 7 GPa) for samples with low FeO contents (<7.5 wt%) (Fig. 9).

By contrast, samples with higher FeO contents (>7.5 wt%) were derived from similar depths, but these correspond to pressures that exceed by several GPa the apparent depths at which they lost a partial melt (~2 to 3 GPa). Herzberg (1999) explained the paradoxical observation that many high-temperature (FeO-rich) xenoliths are derived from pressures >5 GPa, but appear to have formed as residues from melting at pressures <3 GPa, in terms of a model of melt depletion at shallow pressures followed by underthrusting.

The possibility that peridotites from Lac de Gras with relatively high FeO contents represent residues from melting at low pressures, which were subsequently subducted to greater depths, cannot be discounted. However, these samples are part of a trend that grades into samples with FeO contents higher than the primitive mantle and which therefore are not simple melt residues. This makes it likely that many if not all of these deep FeO-rich peridotites have suffered secondary re-enrichment in FeO (as

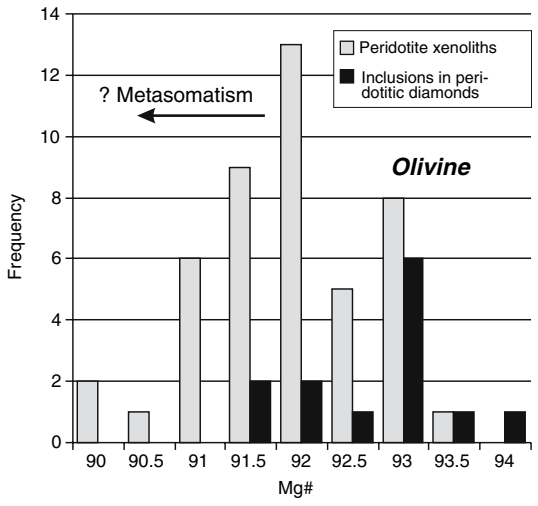

Fig. 7 Mg# in olivines from peridotite xenoliths compared to olivine inclusions in peridotitic diamonds (Davies et al. 1999, 2004) from the Lac de Gras kimberlites. Lower Mg-numbers in xenolithic olivine may be due to metasomatic Fe enrichment

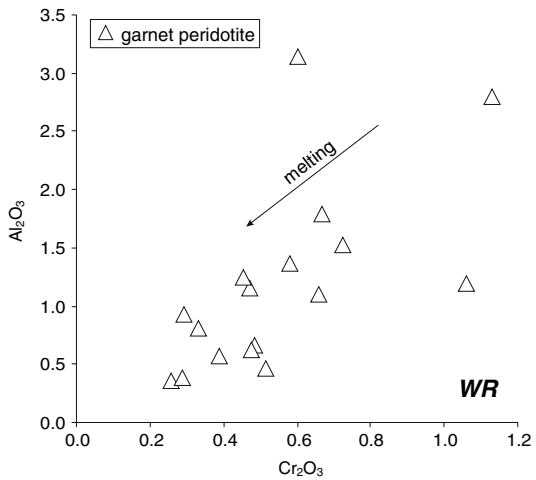

Fig. 8 Cr_2O_3 against Al_2O_3 (wt%) in reconstructed peridotites; a qualitative partial melting trend is also shown

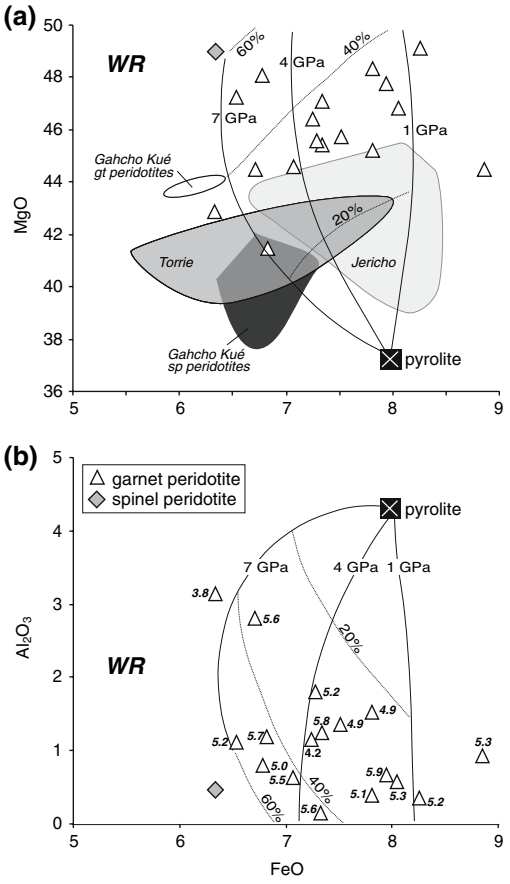

Fig. 9 FeO against **a** MgO and **b** Al_2O_3 (wt%) of reconstructed peridotites compared to experimental residues of isobaric batch melting at different pressures (*solid lines*, GPa) of pyrolite for different degrees of partial melting (*hatchured lines*; Walter 1999); **a** also shown are fields for peridotites from the Jericho kimberlite (north-central Slave Craton; Kopylova et al. 1999), Torrie (between Jericho and Lac de Gras, excluding olivine websterites; MacKenzie and Canil 1999) and Gahcho Kué (southeastern Slave Craton, separated into garnet (*gt*) and spinel (*sp*) peridotites; Kopylova and Caro 2004). Pressures of last equilibration (bold italics, in GPa; P_{NG} at T_{OW79}, Table 8) are given next to *symbols* for peridotites from Lac de Gras in **b**

discussed above). This re-enrichment leads to spuriously low apparent melt depletion pressures. Unless a mantle volume, such as the deep lithospheric mantle layer beneath Lac de Gras, can be a melange of subcreted and subducted lithosphere, we favour a model of plume subcretion because of the clear evidence for >3 GPa melting and the likelihood of secondary FeO addition.

Finally, it should also be noted that stacking of oceanic lithosphere should lead to repetitive sequences of mantle packages, with each grading from less to more FeO-depleted peridotite in the mantle column, whereas a continuous decrease in Mg# with depth is observed for nearly all cratonic mantle sections (Gaul et al. 2000; Griffin et al. 2004).

The spinel harzburgite included in this study is probably derived from a depth shallower than the shallowest garnet peridotite (3.7 GPa), but apparently lost a partial melt at more than 7 GPa. For this sample, a fractional melting model, in which melting starts at 7–3 GPa and continues to 1 GPa, is more successful in reconciling the depths of melting and of entrainment and is consistent with formation of the shallow central Slave lithosphere in a convergent margin setting (Griffin et al. 1999b; Aulbach et al. 2005).

Summary and conclusions

We have investigated the major-element and modal composition of peridotites from the Lac de Gras kimberlites in the central Slave Craton to obtain further constraints on the origin of the deep subcontinental lithospheric mantle in this region. Positive MgO–NiO and negative MgO–CaO correlations, combined with Ca and Al contents lower than those of fertile mantle for many peridotites, are consistent with the extraction of partial melts from these samples. Iron oxide contents exceeding those of the fertile mantle, and a negative correlation between FeO and SiO_2 indicate that secondary processes have affected the mantle, raising its mean FeO content. Some silica-rich, FeO-poor peridotites may have interacted with silica-rich melts. Others may represent primary melt residues formed by peritectic opx production on the solidus. Silica-poor, FeO-rich peridotites may indicate olivine addition (± opx dissolution).

Major-element compositions and modal mineralogies of peridotitic mantle are sensitive to melt extraction pressures (e.g. Herzberg 1995; Walter 1998; Canil 2004), with pressures <3 GPa corresponding to depths of oceanic lithosphere formation, and higher pressures indicative of formation in upwelling plume mantle. It has been argued that high Cr/Al requires previous depletion of the mantle volume in the spinel stability field followed by subduction to deeper mantle levels (Stachel et al. 1998), and that clinopyroxene as opposed to garnet signatures may indicate a shallow (subduction) origin of deep lithospheric mantle (Canil 2004). However, moderately high Cr/Al may also be generated during high degrees of partial melting at high pressures where neither spinel nor garnet are residual phases. High-Al and high-Ca opx in a garnet- and cpx-free rock, which is stable at temperatures near or above the mantle solidus (Canil 1992), may impart cpx-like signatures during partial melting, followed by garnet and cpx exsolution.

Three main observations suggest that the deep mantle beneath the central Slave Craton formed as a residue from high-pressure melting during plume subcretion: (1) Garnet modes in peridotites from Lac de Gras correspond to those expected for melt extraction at 7 GPa, but show no overlap with those expected for melt extraction at 3 GPa. (2) Olivine in many peridotites has Mg# > 92, which indicates

partial melting at 6–3 GPa (Herzberg 1999). (3) Major-element relationships of most FeO-poor (<7.5 wt%) peridotites from the deep mantle layer coincide with those of experimental melting residues at pressures of ~4 to 7 GPa and these broadly agree with their calculated pressures of last equilibration (4.2–5.8 GPa).

A number of peridotites with equilibration pressures >5 GPa have relatively high FeO contents associated with low SiO_2 contents, which could be interpreted in terms of melt depletion at lower pressures (<3 GPa). However, this is ascribed to secular FeO enrichment of the continental mantle lithosphere, which is supported by the higher average Mg# in armoured olivine inclusions in diamonds (92.6) compared to olivine of peridotite xenoliths (91.7) from the same locality.

Acknowledgments We would like to thank C. Lawson for help with EPMA. This work was funded by a Macquarie University International Postgraduate Award and Postgraduate Research Fund (SA), by an ARC SPIRT grant sponsored by Kennecott Canada Inc., and by ARC Large and Discovery Grants to WLG and SYO'R. Analytical data were obtained using instrumentation funded by ARC LIEF, and DEST Systemic Infrastructure Grants and Macquarie University. Reviews by Dante Canil and Maya Kopylova significantly improved this contribution and editorial handling by Tim Grove is gratefully acknowledged. This is publication number no. 469 from the ARC National Key Centre for Geochemical Evolution and Metallogeny of Continents (http://www.es.mq.edu.au/GEMOC/).

References

Abbott DH, Drury R, Mooney WD (1997) Continents as lithological icebergs: the importance of buoyant lithospheric roots. Earth Planet Sci Lett 149:15–27

Aulbach S, Griffin WL, Pearson NJ, O'Reilly SY, Kivi K (2004) Mantle formation and evolution, Slave Craton: constraints from HSE abundances and Re–Os isotope systematics of sulfide inclusions in mantle xenocrysts. Chem Geol 208:61–88

Aulbach S, Griffin WL, Pearson NJ, O'Reilly SY, Kivi K. (2005) Os-Hf-Nd isotope constraints on subcontinental lithospheric mantle evolution, Slave Craton (Canada). Geochim Cosmochim Acta 69(Suppl):284

Bleeker W (2003) The late Archean record: a puzzle in ca. 35 pieces. Lithos 71:99–134

Bleeker W, Ketchum JWF, Jackson VA, Villeneuve M (1999) The central Slave Basement cComplex. Part I: Its structural topology and autochthonous core. Can J Earth Sci 36:1083–1109

Bostock MG (1998) Mantle stratigraphy and evolution of the Slave province. J Geophys Res 103:21183–21200

Boyd FR (1997) Correlation of orthopyroxene abundance with the Ni content of coexisting olivine in cratonic peridotites (abstract). Trans Am Geophys Union, Fall Meeting Abstract Volume, F746

Boyd FR, McCallister RH (1976) Densities of fertile and sterile garnet peridotites. Geophys Res Lett 3:509–512

Boyd FR, Pokhilenko NP, Pearson DG, Mertzman SA, Sobolev NV, Finger LW (1997) Composition of the Siberian cratonic mantle: evidence from Udachnaya perioditite xenoliths. Contrib Mineral Petrol 128:228–246

Brey GP, Köhler T, Nickel KG (1990) Geothermobarometry in 4-phase lherzolites. 1. Experimental results from 10 to 60 KB. J Petrol 31:1313–1352

Canil D (1991) Experimental evidence for the exsolution of cratonic peridotite from high-temperature harzburgite. Earth Planet Sci Lett 106:64–72

Canil D (1992) Orthopyroxene stability along the peridotite solidus and the origin of cratonic lithosphere beneath southern Africa. Earth Planet Sci Lett 111:83–95

Canil D (2004) Mildly incompatible elements in peridotites and the origins of mantle lithosphere. Lithos 77:375–393

Carbno GB, Canil D (2002) Mantle structure beneath the SW Slave Craton, Canada: constraints from garnet geochemistry in the Drybones Bay Kimberlite. J Petrol 43:129–142

Cook FA, van der Velden AJ, Hall KW, Roberts BJ (1999) Frozen subduction in Canada's Northwest Territories: lithoprobe deep lithospheric reflection profiling of the western Canadian shield. Tectonics 18:1–26

Cox KG, Smith MR, Beswetherick S (1987) Textural studies of garnet lherzolites: evidence of exsolution origin from high temperature harzburgites. In: Nixon PH (ed) Mantle Xenoliths. Wiley, London, pp 537–550

Davies RM, Griffin WL, Pearson NJ, Andrew AS, Doyle BJ, O'Reilly SY (1999) Diamonds from the deep: Pipe DO-27, Slave Craton, Canada. In: Gurney JJ, Gurney JL, Pascoe, MD, Richardson SH (eds) Proceedings of 7th international Kimb Conf, Red Roof Design cc, Cape Town, pp 148–155

Davies RM, Griffin WL, O'Reilly SY, Doyle BJ (2004) Mineral inclusions and geochemical characteristics of microdiamonds from the DO27, A154, A21, A418, DO18, DD17 and Ranch Lake kimberlites at Lac de Gras, Slave Craton, Canada. Lithos 77:39–55

Davis WJ, Hegner E (1992) Neodymium isotopic evidence for the tectonic assembly of Late Archean crust in the Slave Province, northwest Canada. Contrib Mineral Petrol 111:493–504

Davis WJ, Jones AG, Bleeker W, Grutter H (2003) Lithosphere development in the Slave Craton: a linked crustal and mantle perspective. Lithos 71:575–589

Droop G (1987) A general equation for estimating Fe3+ concentrations in ferromagnesian silicates and oxides from microprobe analyses, using stoichiometric criteria. Geol Mag 51:431–435

Gaul OF, Griffin WL, O'Reilly SY, Pearson NJ (2000) Mapping olivine composition in the lithospheric mantle. Earth Planet Sci Lett 182:223–235

Griffin WL, O'Reilly SY, Ryan CG (1999a) The composition and origin of subcontinental lithospheric mantle. In: Fei Y, Bertka CM, Mysen BO (eds) Mantle petrology: field observations and high-pressure experimentation. Spec Publ, The Geochemical Society, Washington, pp 13–45

Griffin WL, Doyle BJ, Ryan CG, Pearson NJ, O'Reilly SY, Natapov LM, Kivi K, Kretschmar U, Ward J (1999b) Lithosphere structure and mantle terranes: Slave Craton, Canada. In: Gurney JJ, Gurney JL, Pascoe MD, Richardson SH (eds) Proceedings of 7th international Kimb conference red roof design cc, Cape Town, pp 299–306

Griffin WL, O'Reilly SY, Doyle BJ, Pearson NJ, Coopersmith H, Kivi K, Malkovets V, Pokhilenko N (2004) Lithosphere mapping beneath the North American plate. Lithos 77:873–922

Grütter HS, Apter DB, Kong J (1999) Crust-Mantle Coupling: Evidence from mantle-derived xenocrystic garnets. In: Gurney JJ, Gurney JL, Pascoe MD, Richardson SH (eds) Proceedings of 7th international Kimb Conference, red roof design cc, Cape Town, pp 307–312

Gurney J (1984) A correlation between garnets and diamonds in kimberlites. Publs Geol Dept& Univ Extension. Univ West Aust 8:143–166

Gurney JJ, Harte B (1980) Chemical variations in upper mantle nodules from southern African kimberlites. Phil Trans Roy Soc Lond A297:273–293

Herzberg C (1995) Generation of plume magmas through time—an experimental perspective. Chem Geol 126:1–16

Herzberg CT (1999) Phase equilibrium constraints on the formation of cratonic mantle. In: Fei Y, Bertka CM, Mysen BO (eds) Mantle petrology: field observations and high-pressure experimentation. Spec Publ, The Geochemical Society, Washington, pp 241–257

Irvine GJ, Pearson DG, Kjarsgaard BA, Carlson RW, Kopylova MG, Dreibus G (2003) A Re–Os isotope and PGE study of kimberlite-derived peridotite xenoliths from Somerset Island and a comparison to the Slave and Kaapvaal cratons. Lithos 71:461–488

Jordan TH (1988) Structure and formation of the continental tectosphere. J Petrol Spec 29:11–38

Kelemen PB, Hart SR, Bernstein S (1998) Silica enrichment in the continental upper mantle via melt/rock reaction. Earth Planet Sci Lett 164:387–406

Kinzler RJ, Grove TL (1999) Origin of depleted cratonic Harzburgite by deep fractional melt extraction and shallow olivine cumulate infusion. In: Gurney JJ, Gurney JL, Pascoe, MD, Richardson SH (eds) Proceedings of 7th international Kimb conference, red roof design cc, Cape Town, pp 437–443

Kopylova MG, Caro G (2004) Mantle Xenoliths from the Southeastern Slave Craton: evidence for chemical zonation in a thick, cold lithosphere. J Petrol 45:1045–1067

Kopylova MG, Russell JK, Cookenboo H (1999) Petrology of peridotite and pyroxenite xenoliths from the Jericho kimberlite: implications for the thermal state of the mantle beneath the Slave Craton, Northern Canada. J Petrol 40:79–104

Kusky TM (1989) Accretion of Archean slave province. Geology 17:63–67

MacKenzie JM, Canil D (1999) Composition and thermal evolution of cratonic mantle beneath the central Archean Slave province, NWT, Canada. Contrib Mineral Petrol 134:313–324

Menzies MA, Hawkesworth CJ (1987) Upper mantle processes and composition. In: Nixon PH (ed) Mantle Xenoliths. Wiley, Chichester, pp 725–738

Menzies A, Westerlund K, Grütter H, Gurney J, Carlson J, Fung A, Nowicki T (2004) Peridotitic mantle xenoliths from kimberlites on the Ekati Diamond Mine property, N.W.T., Canada: major element compositions and implications for the lithosphere beneath the central Slave Craton. Lithos 77:395–412

Nickel KG, Green DH (1985) Empirical geothermobarometry for garnet peridotites and implications for the nature of the lithosphere, Kimberlites and Diamonds. Earth Planet Sci Lett 73:158–170

Nisbet EG, Cheadle MJ, Arndt NT, Bickle MJ (1993) Constraining the potential temperature of the Archaean mantle; a review of the evidence from komatiites. Lithos 30:291–307

Norman MD (1998) Melting and metsomatism in the continental lithosphere: laser ablation ICPMS analysis of minerals in spinel lherzolites from eastern Australia. Contrib Mineral Petrol 130:240–255

O'Neill HSC, Wood BJ (1979) An experimental study of the iron–magnesium partitioning between garnet and olivine and its calibration as a geothermometer. Contrib Mineral Petrol 70:59–70

Pearson NJ, Griffin WL, Doyle BJ, O'Reilly SY, van Achterbergh E, Kivi K (1999) Xenoliths from kimberlite pipes of the Lac de gras area, Slave Craton, Canada. In: Gurney JJ, Gurney JL, Pascoe, MD, Richardson SH (eds) Proceedings of 7th international Kimb conference, red roof design cc, Cape Town, pp 644–658

Poudjom Djomani YH, Griffin WL, O'Reilly SY, Doyle BJ (2005) Lithospheric domains and controls on kimberlite emplacement, Slave Province, Canada: evidence from elastic thickness and upper mantle composition. Geochem Geophys Geosyst 6: Art. No. Q10006

Ringwood AE (1975) Composition and petrology of the earth mantle. McGraw Hill, New York

Shirey S, Richardson SH, Harris JW (2004) Integrated models of diamond formation and craton evolution. Lithos 77:923–944

Smith D, Boyd FR (1987) Compositional heterogeneities in a high-temperature lherzolite nodule and implications for mantle processes. In: Nixon PH (ed) Mantle xenoliths. Wiley, New York, pp 551–561

Sobolev N, Lavrent'yev Y, Pokhilenko N, Usova L (1973) Chrome-rich garnets from the kimberlites of Yakutia and their paragenesis. Contrib Mineral Petrol 40:39–52

Solomon M (1963) Counting and sampling errors in modal analysis by point counter. J Petrol 4:367–382

Stachel T, Viljoen KS, Brey G, Harris JW (1998) Metasomatic processes in lherzolitic and harzburgitic domains of diamondiferous lithospheric mantle: REE in garnets from xenoliths and inclusions in diamonds. Earth Planet Sci Lett 159:1–12

Stachel T, Harris JW, Tappert R, Brey GP (2003) Peridotitic diamonds from the Slave and the Kaapvaal cratons—similarities and differences based on a preliminary data set. Lithos 71:489–503

Streckeisen A (1976) To each plutonic rock its proper name. Earth Sci Rev 12:1–33

Tappert R, Stachel T, Harris JW, Brey GP (2005) Mineral inclusions in diamonds from the Panda kimberlite, Slave Province, Canada. Eur J Mineral 17:423–440

Walter MJ (1998) Melting of garnet peridotite and the origin of komatiite and depleted lithosphere. J Petrol 39:29–60

Walter MJ (1999) Melting residues of fertile peridotite and the origin of cratonic lithosphere. In: Fei Y, Bertka CM, Mysen BO (eds) Mantle petrology: field observation and high pressure experimentation, The Geochemical Society, Spec Publ, pp 225–239

Walter MJ (2004) Melt extraction and compositional variability in mantle lithosphere. In: Holland HD, Turekian KK, Carlson, RW (eds) Treatise on Geochemistry, vol 2: The Mantle and the Core. Elsevier Pergamon, Amsterdam, pp 363–394

Westerlund KJ, Shirey SB, Richardson SH, Carlson RW, Gurney JJ, Harris JW (2006) A subduction wedge origin for PaleoArchean peridotitic diamonds and harzburgites from the Panda kimberlite, Slave Craton, evidence from Re–Os isotope systematics. Contrib Mineral Petrol 152:275–294